

Dynamic analysis of lightly iced conductor galloping in two degrees of freedom

A.S. Richardson, Jr., B.Sc., M.Sc., Sen. Mem. I.E.E.E.

Indexing terms: Cables and overhead lines, Power transmission, Power systems and plant

Abstract: Field observations have been repeatedly reported on the galloping of transmission lines having only a small accretion of ice of the order of 10% of the diameter on the windward side. Aerodynamic force measurements in wind tunnels reveal that significant lift forces are present, having a steep gradient with respect to angle of attack, and which satisfy the Den Hartog negative damping criteria. Drag forces are essentially constant, and aerodynamic moments are zero over the 360° range of angle of attack. Similarly, no unbalanced inertia forces exist for such light-ice deposits, which precludes the dynamic inertia coupling between galloping and torsion modes.

Blow back of the conductor is shown to explain such galloping owing to the angle of attack reaching the critical range, within a finite range of wind speed. The addition of control devices, identified as the winddamper, and the detuner, is shown to modify the distribution of angle of attack along the span, thus altering the angle of attack 'exposure' compared with that of an untreated span. Stability analyses in two degrees of freedom (galloping and dynamic twist) are performed for a number of representative cases. Stability is expressed as the root locus of a fourth-degree polynomial (quartic) equation, as a function of wind speed. Perforated cylinder dampers are also considered, and they are found to supply inadequate damping for control, unless the span coverage is unreasonably large. The twisting effect of the Winddamper is shown to be its primary stabilising influence. The detuner appears to increase the range of instability in two out of three cases.

List of symbols

C_L	= lift coefficient (dimensionless, based on conductor diameter)
$C_{L\alpha}$	= lift coefficient slope with angle of attack
α	= local angle of attack
C_D	= drag coefficient (dimensionless, based on conductor diameter)
C_α	= Den Hartog coefficient ($C_D + C_{L\alpha}$)
β_0	= blow-back angle, untreated span (eqn. 1), rad
β	= blow-back angle, treated span (eqn. 2), rad
q	= dynamic pressure of wind
d	= conductor diameter
mg	= conductor weight per unit of span length
g	= acceleration due to gravity
U	= wind speed
ρ	= air density
D_1	= aerodynamic drag of damper
W_1	= deadweight of control device
l	= semispan length of conductor span
M	= control device mass
I	= control device moment of inertia about conductor axis
GJ	= torsion stiffness of conductor per unit span length
a	= distance of device CG from conductor axis
θ	= blow-out angle of winddamper (Fig. 7)
K_θ^*	= winddamper aerodynamic stiffness
$d\Sigma/d\theta$	= slope of winddamper moment parameter (Fig. 8)
Σ	= moment parameter for winddamper
ϕ	= dynamic twist angle (Fig. 9)
ω_ϕ	= natural torsion frequency of device, rad/s
ξ_ϕ	= damping in torsion for winddamper
y	= vertical amplitude of galloping mode
ω_y	= natural frequency of galloping mode, rad/s
x	= span co-ordinate measured from midspan
f_y	= mode-shape function of galloping mode
ξ_y	= aerodynamic damping ratio of galloping mode
ξ_0	= damping ratio of galloping mode at zero airspeed
U_c	= critical galloping wind speed

C'_α	= effective spanwise Den Hartog coefficient
ξ_D^*	= effective span damping ratio for device
C_α^*	= Den Hartog coefficient for damper, based on damper area
ξ	= sum of aerodynamic damping ratios
x_θ	= dimensionless eccentric moment coupling parameter
Z	= characteristic length parameter based on dynamic pressure
s_θ	= dimensionless eccentric moment coupling parameter
R	= ratio of torsion to galloping natural frequencies
$C'_{L\alpha}$	= effective spanwise lift coefficient slope
f_ϕ	= torsion mode shape function along span
$C_{L\alpha}^*$	= lift curve slope of damper, based on damper area
r	= span cover factor for aerodynamic damper
t	= time, s
v_y	= eigenvector in y due to ϕ
v_ϕ	= eigenvector in ϕ due to y

1 Introduction

Recent developments in the field of galloping-conductor technology have encompassed a wide spectrum of engineering and practical approaches. A new reference book [1] includes an up-to-date summary of a number of methods that have been applied, mainly on an experimental basis, during the past 15 years. These methods include electrical permutation of circuits [2], unbundling of bundled conductors [3], interphase spacers [4], and the application of several device concepts for galloping control [5, 6, 7].

In addition, advances have been made in the theoretical approach to galloping. Some of these have concerned the maximum possible galloping amplitude [8], and have resulted in very crude predictions of amplitude dependency on wind speed. That particular theory is based on energy-balance principles, but also aerodynamic nonlinear coefficients of lift in the range bounded by ± 0.6 as in a step function. Although that characterisation is greatly different from the wind-tunnel measurements of lift coefficient on 'typical' ice-shaped models, the maximum reported galloping amplitudes by the EEI Galloping Task Force in 66 reported cases exceed the value calculated by the theory [8] in only 9% of the cases [1]. It appears that the compelling simplicity of this result should guarantee its continued usage. However, the theory seems to break down when it is applied to aerodynamic dampers,

Paper 1379C, first received 20th May and in revised form 25th November 1980

The author is with Research Consulting Associates, 3 Wingate Road, Lexington, MA 02173, USA

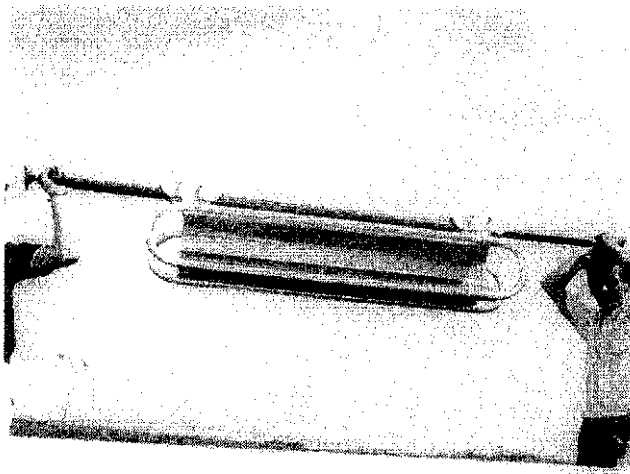


Fig. 1 Winddamper

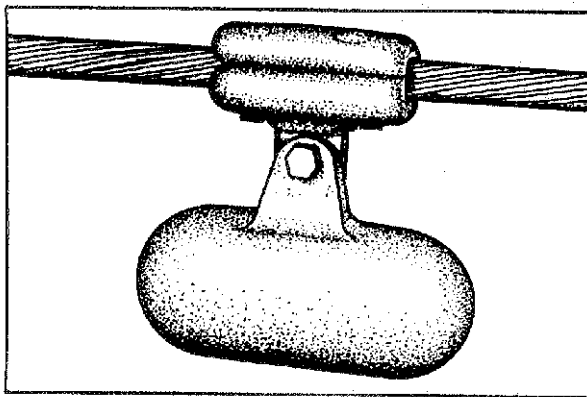


Fig. 2 Detuner pendulum

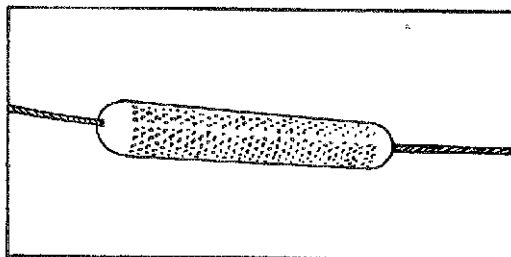


Fig. 3 Perforated cylinder damper

predicting only modest reduction in galloping amplitudes, whereas field observations indicate significantly reduced amplitudes [9]. One objective of this paper is to explain why this is so.

Another theory which has appeared within the past five years is the torsional 'detuning' theory. Here, the fundamental notion is that a matching of the conductor torsional mode frequency with one of the lower galloping mode frequencies due to ice and wind effects is the cause of galloping [10]. In the detuning theory a remedy is proposed for control, consisting of a discrete number of 'detuner pendulums' that are to be attached along the span. One puzzling aspect of this theory is that it cannot be reconciled with the predominance of galloping cases reported under lightly iced conductors [1], where ice thickness is less than 0.25 cm. For such light-ice coatings the effects on the conductor torsion natural frequency are negligibly small, as are the effects of the static unbalance due to ice. The mechanism for coupling between torsion and galloping in such cases is nonexistent in single conductors, and

in bundled conductors is difficult to visualise even though, in the latter, the torsion and galloping frequencies may be almost matched. Yet this method has received such widespread attention that an in-depth analysis of it seems warranted. That is a second objective of the paper.

The final theory, which is the primary objective of the paper, is one based on the original Den Hartog theory, but including the effects of spanwise twisting [11]. Here, that theory will be extended to include the coupled motions of torsion and galloping, especially due to the added control devices. No nonlinearities are considered. Stability or instability is judged solely on the basis of the sign of the mode damping ratio: stable if positive, unstable if negative. Here, the mode damping ratio is found from the solution of a quartic equation, whose roots are the eigenvalues for the coupled system. In control theory terminology, the question is: are there any poles (roots) in the left half plane?

As a practical matter, and to illustrate the method, a typical conductor span of Drake single conductor on 277 m span at 20% UBS* tension is considered subject to a coating of light ice. The untreated span is compared to treated spans, having, in turn, detuner pendulums, perforated cylinder dampers, and windampers. Attachment points, in all cases, are the two one-third points in the span. For a consistent comparison, detuner and winddamper eccentric mass and moment of inertia are equal, and perforated cylinder damper and winddamper drag are equal up to 64 km/h wind speed.

Three initial orientations of the light-ice shape are considered. One with $\alpha_0 = 0$ corresponds to ice accretion directly to windward. The other two, having $\alpha_0 = 10^\circ$ and $\alpha_0 = -10^\circ$, respectively, refer to ice accretion slightly above or slightly below a horizontal plane.

Although the developed theory is applied to a specific illustrative example, the notation is generalised to afford application to any single-conductor problem having a light-ice profile.

2 Description of conductor used for the illustration of the method

The standard Drake conductor (54/7 ACSR) is used to illustrate the necessary considerations, see Table 1.

Table 1: Conductor specification

Type:	54/7 ACSR	Drake 795 MCM
Overall diameter =	1.093 in	(27.76 mm)
UBS =	28 500 lbs	(12,950 kgf)
Weight =	1.09 lb/ft	(1.61 kg/m)
Torsion stiffness =	1045 lbft ² /rad	(432 Nm ² /rad)
Tension =	5,800 lb	(2636 kgf)
Span =	900 ft	(277 m)
Moment of inertia =	0.17 lbm ² /ft	(1.65 kgcm ² /m)
Sag =	19 ft	(5.85 m)
1st mode frequency =	0.23 Hz	(1.44 rad/s)
2nd mode frequency =	0.46 Hz	(2.88 rad/s)

3 Initial conditions with light ice

The entire span is assumed to be coated with light ice having a thickness of 0.1 in (0.25 cm), and a crescent shape formed on the windward side. The aerodynamic characteristics were found in wind-tunnel tests [12], and also later reported in a CIGRE paper [13]. For the purpose of analysis, the drag coefficient is assumed constant at a value of unity, the moment coefficient is assumed zero, and the lift coefficient C_L , the lift coefficient slope $C_{L\alpha}$, and the Den Hartog coefficient, $C_\alpha = C_D + C_{L\alpha}$ are represented by analytical approximation [11]. The latter two, used in the present analysis, are indi-

UBS = ultimate breaking strength

cated in Fig. 4. The angle of attack, measured positive clockwise with the wind from the left, is considered as zero when the axis of symmetry of the crescent is in a horizontal plane. Both the C_{α} function and the $C_{L\alpha}$ function are even functions of α . For an angle of attack greater than 40° , $C_{\alpha} = C_D = 1.0$

Notice that the C_{α} function can reach positive values of +3, but the negative limit is -1. This comes into play in a twisted conductor, and has a profound effect on the stability of the span.

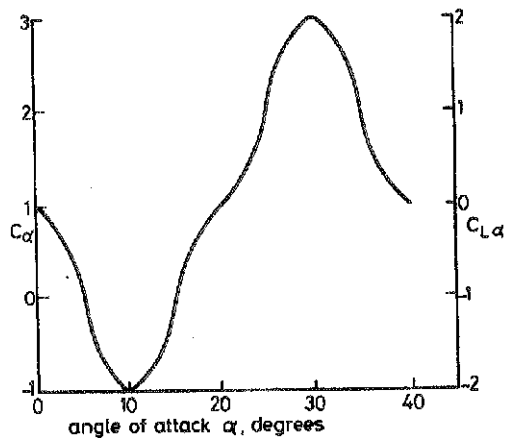


Fig. 4 Aerodynamic coefficients for light ice

Because the ice coating is light, no change is assumed in the conductor polar moment of inertia, and the aerodynamic moment is considered zero. The angle of attack range in which C_{α} is negative is from 5° and 15° . The ice shape can reach this condition (and may become unstable) when the conductor blow-back angle β_0 comes within that range. For small angles,

$$\beta_0 = C_D q d / mg \quad (1)$$

where

d = conductor diameter

q = dynamic wind pressure ($\rho U^2 / 2$)

ρ = air density = 1.23 kg/m^3

U = wind speed

mg = conductor weight per unit length

For the Drake conductor, the blow back at 32 km/h wind speed is about 4.8° , which is in the stable range of C_{α} . At 40 km/h the blow back is 7.5° , and, since C_{α} is negative, the conductor may gallop. If the initial angle α_0 of ice formation is different from zero, then different wind speeds are required to reach the range of negative values. Further, the addition of certain types of control devices will change the blow-back picture somewhat.

In the case of either the Winddamper or the perforated cylinder the blow back is*

$$\beta = [\beta_0 + (4/3)(D_1/mgl)] / [1 + (8/3)W_1/mgl] \quad (2)$$

where

D_1 = aerodynamic drag of device

l = semispan length

W_1 = weight of device

For comparison purposes, the perforated cylinder is assumed to have the same drag as the winddamper, and the same weight.

*The catenary is assumed to have a parabolic shape.

Also both are assumed located at each of the one-third span points.

The latest version of the perforated cylinder has a length of 3.05 m and a mass per unit length of 3.52 kg/m [14]. This compares on an equal weight basis with a 1.2 m - length winddamper. The comparison on the basis of drag is also correct if it may be assumed that the perforated cylinder develops a drag coefficient of 1.15, as against the drag coefficient of the winddamper of 2.15.

In the case of the detuner pendulum, there is no drag, but the weight is assumed equal to that of the winddamper, i.e. 22 lb (10 kg).

The blowback is shown in Fig. 5 for the various cases to be considered. In the case of the perforated cylinder damper, it is assumed here to be attached concentrically with the single conductor axis. This is somewhat at variance with the use it has seen on bundled conductor to date, but, in the present comparison, the use of a little imagination could interpret the results for it in terms of a bundled-conductor application as well. No bundled-conductor applications are considered here for either the winddamper or the detuner pendulum, however.

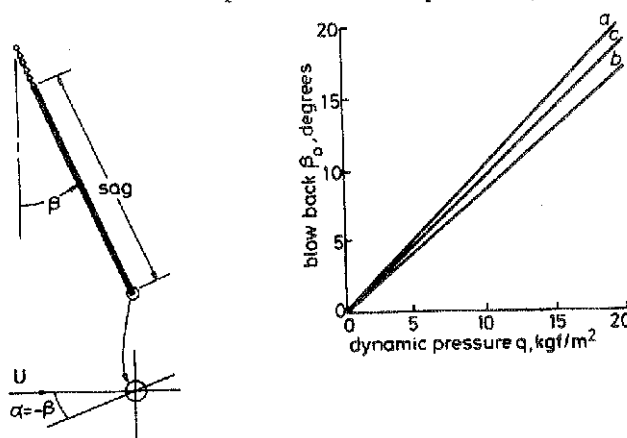


Fig. 5 Conductor blow-back angle

a Winddamper and cylinder
b Detuner pendulum
c Untreated span

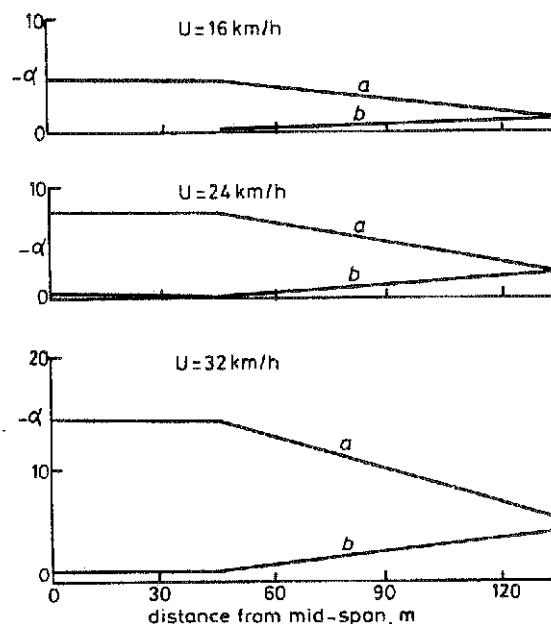


Fig. 6 Angle of attack distribution along span for winddamper and detuner

a Winddamper b Detuner
Total span = 274 m; Drake conductor; 1/3 span attachment for device units
Axis of symmetry of ice shape is initially horizontal ($\alpha_0 = 0$)

It is seen that the dead weight of the units reduces the blow back by approximately 12%, but the aerodynamic units tend to increase the blow back according to dynamic wind pressure. At a wind speed of 40 km/h the blow-back angles are 6.7° for the detuner, 7.5° for the untreated span, and 8.3° for the aerodynamic units. However, there is more to consider.

As the conductor blows back with the devices attached to the one-third span points, the offset pendulum weight applies a twisting moment which twists the conductor, clockwise according to our convention, thus limiting the angle-of-attack change due to blow back. On the other hand, the windamper by its action twists the conductor in a counterclockwise direction, thus increasing the angle-of-attack change locally. Contrary to this, the perforated cylinder just blows back with the conductor, the angle of attack being $\alpha = -\beta$, and constant along the span. The angle of attack distributions along the semispan for the windamper and the detuner pendulum are shown in Fig. 6, for three wind speeds. These are symmetrical about midspan. In the case of the windamper, the centre one-third span blows out according to Fig. 7 [11].

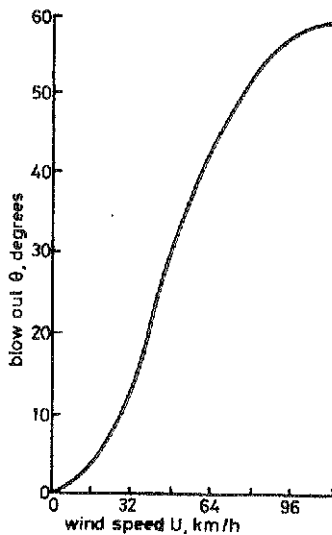


Fig. 7 Windamper blow out for Drake conductor

4 Dynamic twisting

As a part of establishing initial conditions, the dynamic twisting, including the effects of the devices, must be established.

There are two modes to consider:

(a) in-phase twisting when the devices located at the one-third points move in phase with each other

(b) out-of-phase twisting when the devices move in anti-phase.

The latter has the higher frequency.

Zero air speed case: When there is no wind, the dynamic twisting of the windamper and the detuner pendulum are identical. Also, it is easily established that the kinetic energy of the twisting conductor mass is less than 1% of the kinetic energy of the moving devices except when the devices form a nodal point, the latter being the third torsion mode having a frequency outside the range of concern. Accordingly, the in-phase mode natural frequency is given by eqn. 3a, and the out-of-phase, natural frequency by eqn. 3b:

$$\omega_{\phi} = \sqrt{\frac{Mga + GJ/2l/3}{I}} \quad (3a)$$

$$= \sqrt{\frac{Mga + GJ/2l/3 + GJ/1l/3}{I}} \quad (3b)$$

where

Mg = device weight (10 kg)

I = device moment of inertia about conductor

GJ = conductor torsion stiffness

a = distance from device CG to conductor

The calculated frequencies are 6.11 rad/s and 6.95 rad/s, respectively.

Effect of wind: There is no effect of wind on the detuner natural frequencies, but there will be an effect on the windamper owing to the blow out of it and the aerodynamic stiffness of it. The blow out effect is accounted for by replacing Mga by $Mga \cos \theta$, and θ varies as in Fig. 7. The aerodynamic stiffness is accounted for by the sigma parameter [11] shown in Fig. 8. This results in an 'effective' stiffness for the windamper amounting to

$$K_{\theta}^* = -aqd\Sigma/d\theta \quad (4)$$

In this expression the slope of the sigma curve is a function of the wind speed.

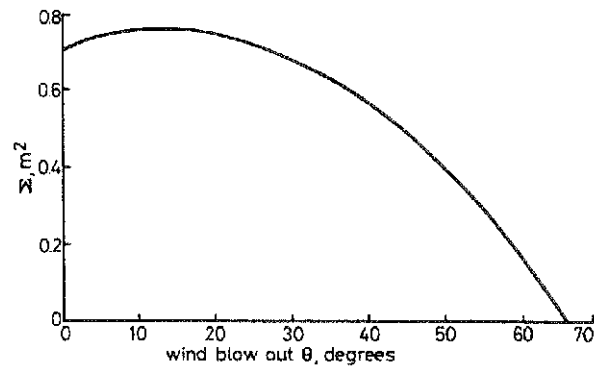


Fig. 8 Aerodynamic moment parameter Σ (1.2 m damper)

The torsion natural frequencies, including the 'effective' windamper stiffness, are shown in Table 2. The first column shows the in-phase frequencies, and the second shows the out-of-phase frequencies. Notice a slight reduction in numerical value at low wind speed corresponding to the positive slope of the sigma parameter for small blow-out angles, Fig. 8.

Table 2: Windamper torsion frequencies

Wind speed	Frequency		K_{θ}^*
km/h	rad/s		m/rad
0	6.11	6.95	-1.33
16	5.99	6.85	-0.80
24	6.04	6.89	+2.66
32	6.34	7.15	10.00
40	6.95	7.70	20.93
48	7.76	8.44	34.26
56	8.65	9.27	53.33
64	9.79	10.33	82.26
72	11.29	11.77	112.26

In the case of the detuner, the frequencies are constant at the zero wind speed values.

With reference to Fig. 9, dynamic twisting motion ϕ is considered, first, without any coupling to the y co-ordinate and governed by the differential equation

$$I\ddot{\phi} + I\omega_{\phi}^2\phi = qa d\Sigma/d\theta (a\dot{\phi}/U) \sin \theta \quad (5)$$

where the aerodynamic twisting moment on the right-hand side is seen to be proportional to the angular velocity. By

rearranging terms, this may be put into the standard form:

$$\ddot{\phi} + 2\xi_{\phi}\omega_{\phi}\dot{\phi} + \omega_{\phi}^2\phi = 0 \quad (6)$$

where

$$\xi_{\phi} = -qa^2 \sin \theta (d\Sigma/d\theta)/2UI\omega_{\phi}$$

the latter being the damping ratio in the torsion mode. It is seen to be proportional to wind speed, and to the aerodynamic sigma parameter. Since the latter always has negative slope with θ over the range of wind speed of practical interest, the damping is always positive. At 48 km/h the damping ratio is about 2%. In the case of the detuner pendulum, the damping ratio is assumed zero.

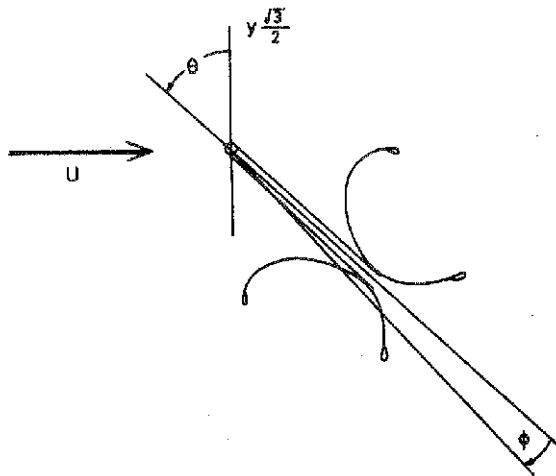


Fig. 9 Generalised co-ordinates

5 Single-degree-of-freedom vertical motion

The differential equation for the uncoupled vertical motion in either the first mode or the second mode is [11, 12]

$$\ddot{y} + \omega_y^2 y = -(qd\dot{y}/mlU) \int_{-1}^1 C_{\alpha} f_y^2 dx \quad (7)$$

where $f_y = \cos(\pi x/2l)$ for the first mode, and $= \sin(\pi x/l)$ for the second mode, d = conductor diameter, and m = mass per unit length. The natural frequency ω_y , is chosen according to the mode number.

In this form, it is assumed that the aerodynamic coefficient C_{α} can vary along the span, as for the case of either the winddamper or the detuner pendulum. In the case of the untreated span or the perforated cylinder damper, it is constant along the span, and the integral in eqn. 7 becomes C_{α} . On rearranging terms, the equation becomes

$$\ddot{y} + 2\xi_y \omega_y \dot{y} + \omega_y^2 y = 0 \quad (8)$$

where the mode damping ratio is

$$\xi_y = (qd/2mlU\omega_y) \int_{-1}^1 C_{\alpha} f_y^2 dx$$

Hence galloping is defined whenever the average weighted aerodynamic coefficient is negative. In general, it is seen that, when C_{α} varies along the span, its integrated weighted average depends on mode number. The form of eqn. 8 is convenient to use when the mechanical damping ξ_0 of the span is known, because it can be added algebraically to ξ_y , resulting in the critical wind speed

$$U_c = -4\xi_0 m \omega_y / \rho d C_{\alpha}' \quad (9)$$

and C_{α}' is defined as the integrated weighted average of C_{α} .

and ρ = air density

$$C_{\alpha}' = (1/l) \int_{-1}^1 C_{\alpha} f_y^2 dx \quad (10)$$

In the case of either the winddamper or the detuner pendulum, it has already been seen how the angle of attack varies along the span as in Fig. 6. This is used with Fig. 4 to obtain the distribution of the C_{α} coefficient along the span, then weighted according to eqn. 10. In the case of the untreated span or the perforated cylinder damper, since $\alpha = -\beta$ then eqn. 10 reduces to $C_{\alpha}' = C_{\alpha}(-\beta)$.

In the case of either the winddamper or the perforated cylinder damper, there is an additional term to consider in eqn. 8 that is additive to the second term and may be identified by the damping ratio of the damper itself,

$$\xi_D = (3/4)q C_{\alpha}^* A_w / 2ml\omega_y U \quad (11)$$

where

C_{α}^* = aerodynamic coefficient of the damper

A_w = total projected area of all dampers

The factor of 3/4 appears owing to the location of the damper at the one-third points (see Fig. 9). The total area of all dampers used in the span follows from the form of eqn. 7, and the application of the integral to the damper at the appropriate span location.

In the case of the winddamper, at 48 km/h the damping ratio according to eqn. 11 is about 2% in the first mode and 1% in the second, based on a numerical value of C_{α}^* of 3.65 [11]. In the case of the perforated cylinder damper, C_{α}^* is just equal to its drag coefficient of 1.15, but its projected area is 2.5 times that of the winddamper, resulting in first- and second-mode damping ratios of 1.6% and 0.8%, respectively, at 48 km/h. As the span mechanical damping ratio is probably

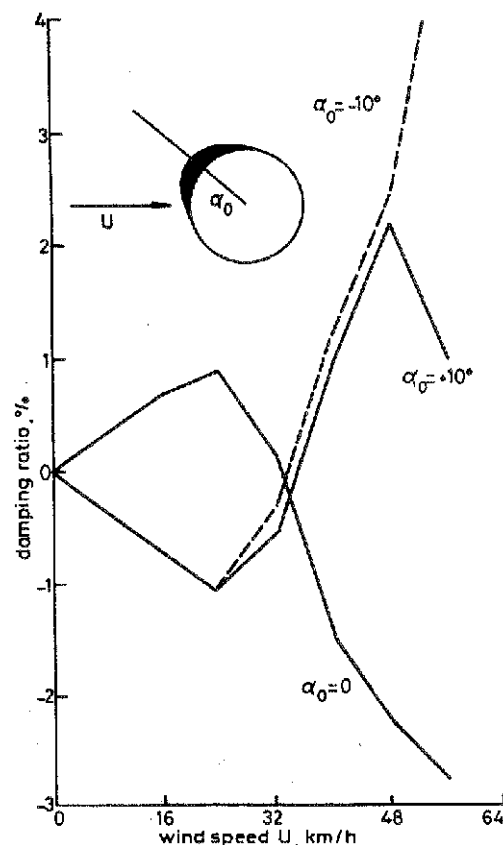


Fig. 10 Untreated span damping ratio: second mode